# RSC Advances



This is an *Accepted Manuscript*, which has been through the Royal Society of Chemistry peer review process and has been accepted for publication.

Accepted Manuscripts are published online shortly after acceptance, before technical editing, formatting and proof reading. Using this free service, authors can make their results available to the community, in citable form, before we publish the edited article. This Accepted Manuscript will be replaced by the edited, formatted and paginated article as soon as this is available.

You can find more information about *Accepted Manuscripts* in the **Information for Authors**.

Please note that technical editing may introduce minor changes to the text and/or graphics, which may alter content. The journal's standard <u>Terms & Conditions</u> and the <u>Ethical guidelines</u> still apply. In no event shall the Royal Society of Chemistry be held responsible for any errors or omissions in this *Accepted Manuscript* or any consequences arising from the use of any information it contains.



Synthesis, Electron Microscopy and Anti-Microbial Property of Fe<sub>3</sub>O<sub>4</sub>-Ag Nanotubes

Mahander Pratap Singh, Y. Raghupathy, K. A. Natarajan, Chandan Srivastava\*

Department of Materials Engineering, Indian Institute of Science, Bangalore-560012, India

\*Corresponding author. Tel: +91-80-22932834

E-mail address: csrivastava@materials.iisc.ernet.in (Chandan Srivastava)

**Abstract** 

Electrodeposition was used for synthesizing 200 nm diameter Fe<sub>3</sub>O<sub>4</sub>-Ag nanotubes.

Compositional analysis at the single nanotube level revealed a fairly uniform distribution of

component elements in the nanotube microstructure. As-synthesized Fe<sub>3</sub>O<sub>4</sub>-Ag nanotubes were

superparamagnetic in nature. Electron diffraction revealed the ultrafine nanocrystalline

microstructure of the nanotubes. Effect of Ag on anti-microbial response of the nanotubes was

investigated by comparing the effect of sulphate reducing bacterial (SRB) on Fe<sub>3</sub>O<sub>4</sub>-Ag and

Fe<sub>3</sub>O<sub>4</sub> nanotubes. Fe<sub>3</sub>O<sub>4</sub> nanotubes were also electrodeposited in the present study. It was

observed that the Fe<sub>3</sub>O<sub>4</sub>-Ag nanotubes exhibited good resistance to sulphate reducing bacteria

which revealed the anti-microbial nature of the Fe<sub>3</sub>O<sub>4</sub>-Ag nanotubes.

**Keywords:** Nanotubes, Anti-bacterial behaviour, ferrofluids, Electron Microscopy.

Introduction

Iron containing nano-solids have found potential application in several fields such as

biomedical imaging<sup>1</sup>, biomedical drug delivery and diagnostics<sup>2</sup>, catalysis<sup>3</sup>, ferrofluids<sup>4</sup> etc. With

respect to their application as ferrofluids, iron containing nanosolids are expected to exhibit three

important characteristics: (a) they should be superparamagnetic. This property can inhibit their

agglomeration due to mutual magnetic attraction. Superparamagnetism can be achieved by

decreasing the grain size of ferromagnetic systems to ultrafine sub-10 nm levels<sup>5</sup>, (b) their

geometry should be such that a foreign material can be packed within their volume so that the contained material can be transferred using a magnetic field through a fluid medium. One such geometry is nanotube geometry. This characteristic can be particularly helpful in drug delivery application and (c) they should posses resistance to degradation in the fluid medium. This degradation can be due to various micro-organisms that are present in the fluid medium. One possible way to avoid bio-corrosion is to incorporate Ag into the nano-solids. Ag is well known for its antimicrobial properties<sup>6</sup>.

This work provides an electrochemical based methodology for synthesizing superparamagnetic Fe<sub>3</sub>O<sub>4</sub>-Ag nanotubes with 200 nm diameter and high aspect ratio. This work also illustrates the superior antibacterial property of as-synthesized Fe<sub>3</sub>O<sub>4</sub>-Ag nanotubes by comparing it with the anti-bacterial response of Fe<sub>3</sub>O<sub>4</sub> nanotubes which were also synthesized in this work. Anti-bacterial response of nanotubes was investigated by exposing them to sulphate reducing bacteria (SRB). SRBs are one of the most prevalent bacteria responsible for bio-fouling and also there is no reported study on the establishment of antibacterial and antifouling properties of Ag in the presence of SRBs.

### **Materials and Methods**

*Synthesis of Nanotubes* 

Fe<sub>3</sub>O<sub>4</sub>-Ag and Fe<sub>3</sub>O<sub>4</sub> nanotubes were synthesized by the conventional electrodeposition technique. Anodic alumina membrane having cylindrical pores with an average diameter of 200 nm, a nominal thickness of 60 μm and density of 10<sup>9</sup> pores/cm<sup>2</sup> was used as template for obtaining nanotube morphology. A platinum foil was used as anode. A copper foil attached to the alumina disc using an adhesive tape was used as cathode. A schematic showing the arrangement of electrodes in the electrochemical cell is provided in Fig. 1.

Synthesis of Fe<sub>3</sub>O<sub>4</sub>-Ag nanotubes: Electrolyte used was prepared by dissolving 0.169 g of AgNO<sub>3</sub>, 2.4 g Fe(NO<sub>3</sub>)<sub>3</sub>.9H<sub>2</sub>O, 0.17 g H<sub>3</sub>BO<sub>3</sub> and 1.7 g of CH<sub>4</sub>N<sub>2</sub>S in 100 mL of distilled water. pH of the solution was maintained at 2.5 using NaHCO<sub>3</sub>. A DC current of 4 mA was applied for 15 minutes for electrodeposition which was carried out at ambient temperature.

Synthesis of Fe<sub>3</sub>O<sub>4</sub> nanotubes: Electrolyte used was prepared by dissolving 2.4 g of Fe(NO)<sub>3</sub>, 0.17 g of H<sub>3</sub>BO<sub>3</sub> in 100 mL distilled water. pH of the solution was maintained at 2.5 using NaHCO<sub>3</sub>. A current of 4 mA was applied for 15 minutes for electrodeposition which was carried out at ambient temperature.

After the electrodeposition experiment, the alumina template containing nanotubes was immersed in 1M NaOH solution and left there for 3-4 hours to dissolve the alumina and release the nanowires. As-synthesized nanowires were then washed several times in distilled water for further analysis.

### Characterization

Quanta ESEM scanning electron microscope (SEM) fitted with an energy dispersive spectroscopy (EDS) detector was used to determine the morphology and composition of asdeposited samples. A 300 keV field emission FEI Tecnai F-30 transmission electron microscope (TEM) was used for obtaining bright field images, selected area electron diffraction (SAD) patterns and compositional information from as-synthesized nanotubes. Samples for the TEM based analysis were prepared by drop-drying a highly dilute dispersion of as-synthesized nanotubes on an electron transparent carbon coated Cu grid. Scanning transmission electron microscopy-energy dispersive spectroscopy (STEM-EDS) technique which uses a ~2 nm sized electron probe was used for obtaining compositional line profiles and elemental maps from individual nanotubes. Room temperature magnetic characterization of as-deposited nanotubes

was performed using Lakeshore VSM using an applied field upto 2 Tesla. X-ray photoelectron spectroscopy (XPS) profile was obtained from the as-synthesized samples using AXIS Ultra DLD (KRATOS ANALYTICAL) instrument.

For determining the anti-microbial response, a mixed culture of sulphate reducing bacteria (SRB) containing *DESULFOTOMACULUM nigrificans* and *DESULFOVIBRIO desulfuricans* was used. Postgate medium<sup>7</sup> used for culturing the SRB strains was made up of 10 g of tryptone, 1 g of sodium sulfite, 1 g of sodium sulfate and 0.5 g of ferric citrate dissolved in 1 litre of de-ionised water. Full growth of inoculated SRB in the medium was achieved in four days. After growth, the bacterial cells were separated using filtration. As-synthesized Fe<sub>3</sub>O<sub>4</sub> and Fe<sub>3</sub>O<sub>4</sub>-Ag nanotubes were drop-dried on Cu plates. These plates were then exposed to the medium containing fully grown bacterial cells. Cu plates were withdrawn from the medium after 15 days for microscopic analysis of bio-films. The nanotubes on these plates were sponged all over the surface and rinsed with ethanol. Bacterial count in the medium exposed to the nanotubes on Cu plates was determined using the PETTROF-HAUSSER Cell Counting Chamber (Hemocytometer). Absorbance of the bacterial growth medium was determined using the SYSTRONICS-117 UV-VIS Spectrophotometer at a wavelength of 420 nm in order to confirm bacterial population in the presence and absence of exposure to these nanotubes.

### **Results and Discussion**

A representative SEM micrograph of as-synthesized Fe<sub>3</sub>O<sub>4</sub>-Ag nanotubes is shown in Fig. 2(a). It can be seen that the electrodeposition experiment has produced high yield of uniform diameter nanotubes. Outer diameter of the nanotubes was found to be approximately 200 nm which is expectedly similar to the diameter of the pores in the alumina template. Surface area of the nanotube was calculated to be approximately 12.5 X 10<sup>-6</sup> mm<sup>2</sup>. For calculating the surface

area, length of the nanotube was considered to be 20 um. Compositional analysis of the assynthesized nanotubes using SEM-EDS technique revealed the presence of Fe, Ag and O element in the nanotubes. Relative atomic percentage of Fe and Ag in the nanotube was found to be 85 at% Fe and 15 at% Ag. Representative low and high magnification TEM bright field image of Fe<sub>3</sub>O<sub>4</sub>-Ag nanotubes is shown respectively in Fig. 2(b) and 2(c). Fig. 2(b) reveals a population of uniform diameter nanotubes. Hollow geometry of the nanotubes is clearly visible in the high magnification images in Fig. 2(c). A representative SAD pattern obtained from an agglomerate of nanotubes is shown in Fig 2(d). Presence of broad diffraction rings in the SAD pattern clearly indicates that the nanotubes are polycrystalline with extremely fine grain sizes. Indexing of the SAD pattern clearly revealed the presence of Fe<sub>3</sub>O<sub>4</sub> phase in the nanotubes. The interplanar spacings ('d' spacings) and corresponding crystallographic planes of the Fe<sub>3</sub>O<sub>4</sub> crystal are indicated in Fig. 2(d). The SAD pattern does not reveal diffraction signature corresponding to the pure Ag phase. This indicated mixing of Ag into the Fe<sub>3</sub>O<sub>4</sub> lattice. XPS spectrum obtained from the nanotubes showing  $Ag3d_{5/2}$  and  $Ag3d_{3/2}$  peaks is provided in Fig. 2(e). XPS based analysis revealed that Ag was present in zero valent state in the nanotubes<sup>8</sup>.

STEM-EDS compositional analysis was conducted to investigate the compositional uniformity in the as-synthesized nanotubes. A representative compositional mapping result is shown in Fig. 3(a). The compositional mapping result clearly reveals that all the three component elements are co-present in all the parts of the nanotube microstructure and there is no preferential segregation of any of the component atom(s). To further confirm the compositional uniformity, compositional line profile analysis was conducted across the nanotube diameter. A representative line profile analysis result is shown in Fig. 3(b). Insert in Fig. 3(b) is the STEM image of the nanowire from which the line profile data was obtained. Two important observations that can be

made from Fig 3(b) are: (a) all the three component atoms are present at every analysis point along the nanotube diameter and (b) a non-bell shaped counts vs distance curve is obtained across the nanotube diameter. A fairly flat curve clearly indicates that the volume of the material along the analysis line is fairly constant. For a cylindrical geometry this is only possible if the cylinder is hollow from inside. A filled cylinder would generate a bell shaped counts vs distance (along the diameter) curve as the amount of material will increase towards the center of the cylinder. The compositional line profile analysis further confirmed the hollow nanotube geometry of the electrodeposited mass.

A representative SEM micrograph of as-deposited Fe<sub>3</sub>O<sub>4</sub> nanotubes is provided in Fig. 4(a). It can be seen that the electrodeposition method has produced a high yield of 200 nm diameter nanotubes. SEM-EDS analysis expectedly revealed the presence of only Fe and O in the nanotubes. Representative high and low magnification of TEM bright field image of Fe<sub>3</sub>O<sub>4</sub> nanotubes is shown respectively in Fig. 4(b) and (c). It can be seen in Fig. 4(b) that uniform diameter hollow Fe<sub>3</sub>O<sub>4</sub> nanotubes have formed. Hollow geometry of the nanotubes is clearly visible in the high magnification image in Fig. 4(c). SAD pattern obtained from an agglomerate of nanotubes is shown in Fig 4(d). Presence of broad diffraction rings in the SAD pattern clearly indicates that the nanotubes are polycrystalline with extremely fine grain sizes. Indexing of the SAD pattern clearly revealed the presence of Fe<sub>3</sub>O<sub>4</sub> phase in the nanotubes. The interplanar spacings ('d' spacings) and corresponding crystallographic planes of the Fe<sub>3</sub>O<sub>4</sub> crystal are indicated in Fig. 4(d). Compositional line profile analysis of individual Fe<sub>3</sub>O<sub>4</sub> nanotubes was conducted using the STEM-EDS technique. A representative line profile analysis result is shown in Fig. 4(e). Insert in Fig. 4(e) is the STEM image of the nanowire from which the line profile

data was obtained. It can be observed in Fig. 4(e) that both Fe and O are fairly uniformly distributed across the nanotube diameter.

Magnetic hysteresis loop obtained from as-synthesized Fe<sub>3</sub>O<sub>4</sub>-Ag and Fe<sub>3</sub>O<sub>4</sub> nanotubes are shown respectively in Fig. 5(a) and (b). Both the magnetic hysteresis loops in Fig. 5 are characterized by extremely low magnetic coercivity and no magnetic saturation till 2 tesla field. Both these attributes reveal superparamagnetic nature<sup>10</sup> of the nanotubes. At all values of the applied magnetic field, a decrease in the magnetization value for the Fe<sub>3</sub>O<sub>4</sub>-Ag nanotubes when compared to the magnetization value of the Fe<sub>3</sub>O<sub>4</sub> nanotube confirmed the presence of diamagnetic Ag in the lattice of the Fe<sub>3</sub>O<sub>4</sub> phase in the case of the Fe<sub>3</sub>O<sub>4</sub>-Ag nanotubes.

SEM micrographs of Fe<sub>3</sub>O<sub>4</sub>-Ag and Fe<sub>3</sub>O<sub>4</sub> nanotube film after exposure to the SRB containing medium are shown respectively in Fig. 6(a) and (b). It can be observed that biofilm has formed on both Fe<sub>3</sub>O<sub>4</sub> and Fe<sub>3</sub>O<sub>4</sub>-Ag nanotubes. It is however clearly evident from the SEM micrographs that between the two nanotubes extent of biofilm formation is considerably less in case of the Fe<sub>3</sub>O<sub>4</sub>-Ag nanotubes. Fe<sub>3</sub>O<sub>4</sub> nanotubes are not visible as they are completely covered by the biofilm whereas Fe<sub>3</sub>O<sub>4</sub>-Ag nanotubes are still visible. Representative TEM micrographs of individual Fe<sub>3</sub>O<sub>4</sub>-Ag and Fe<sub>3</sub>O<sub>4</sub> nanotube after exposure to the SRB are shown respectively in Fig. 7(a) and (b). Supporting the SEM observation, Fig. 7 clearly reveals that the amount of biofilm formed on the Fe<sub>3</sub>O<sub>4</sub> nanotubes is considerably greater that the amount of biofilm on the Fe<sub>3</sub>O<sub>4</sub>-Ag nanotubes.

Compositional analysis of the nanotube film after exposure to SRB revealed that the Fe<sub>3</sub>O<sub>4</sub> nanotube film contained greater amount of bacterially reduced sulfide than the sulfide content in the Fe<sub>3</sub>O<sub>4</sub>-Ag nanotube film. Both the above observations strongly indicate that the extent of biofilm formation is higher in case of non-Ag containing nanotubes. Bacterial count in

the solution exposed to Fe<sub>3</sub>O<sub>4</sub>, and Fe<sub>3</sub>O<sub>4</sub>-Ag was determined using a hemocytometer. Bacterial counts were taken from 16 square boxes, 0.25 mm long and 0.1 mm deep. SRB count obtained from the control, solution exposed to Fe<sub>3</sub>O<sub>4</sub> nanotubes, and solution exposed to Fe<sub>3</sub>O<sub>4</sub>-Ag nanotubes respectively were 8.0 x 10<sup>9</sup>, 3.2 x 10<sup>9</sup>, and 1.4 x 10<sup>9</sup> cells/mL respectively. A significant reduction in the SRB count in solution exposed to Fe<sub>3</sub>O<sub>4</sub>-Ag nanotubes when compared to the bacterial count in control and Fe<sub>3</sub>O<sub>4</sub> nanotubes cases clearly illustrated the role of Ag in inhibiting bacterial growth and thus reducing the extent of biofilm growth. Spectrophotometry was also carried out on the control, solution exposed to Fe<sub>3</sub>O<sub>4</sub> nanotubes and Fe<sub>3</sub>O<sub>4</sub>-Ag nanotubes. De-ionized water was used as reference for these measurements. Absorbance values determined were 0.560, 0.425, and 0.300 respectively for the control, Fe<sub>3</sub>O<sub>4</sub> nanotubes and Fe<sub>3</sub>O<sub>4</sub>-Ag nanotubes cases. Lower optical density corresponds to less scattering of light due to lower density of bacteria. This result also clearly indicated the role of Ag in inhibiting the bacterial growth. The above results clearly illustrated the high anti-microbial property of as-synthesized superparamagnetic Fe<sub>3</sub>O<sub>4</sub>-Ag nanotubes.

### **Conclusions**

200 nm diameter Fe<sub>3</sub>O<sub>4</sub>-Ag and Fe<sub>3</sub>O<sub>4</sub> nanotubes were synthesized using the electrodeposition method. Anodic alumina template was used to obtain the nanotube morphology. The electrodeposition condition adopted produced a high yield of uniform nanotubes. Compositional mapping and compositional line profile analysis results clearly indicated a fairly uniform distribution of component elements in the nanotube microstructure for both the cases. SAED pattern indicated that both Fe<sub>3</sub>O<sub>4</sub>-Ag and Fe<sub>3</sub>O<sub>4</sub> nanotube contained randomly oriented ultrafine nano-crystalline grains. Magnetic measurements revealed a superparamagnetic nature for the Fe<sub>3</sub>O<sub>4</sub>-Ag nanotubes. Exposure of the as-synthesized nanotubes

to SRB revealed the role of Ag in inhibiting the microbial growth. The extent of biofilms formation was considerably greater for the non-Ag containing  $Fe_3O_4$  nanotubes.

# Acknowledgement

Authors acknowledge the electron microscopy facilities available at Advanced Facility for Microscopy and Microanalysis (AFMM), Indian Institute of Science, Bangalore, India. The funding from the Science and Engineering Research Board (SERB) Government of India is deeply acknowledged.

# References

- [1] H. B. Na, I. C. Song and T. Hyeon, Adv. Mater. 2009, 21, 2133.
- [2] S. Guo, D. Li, L. Zhang, J. Li and E. Wang, Biomaterials 2009, 30(10), 1881.
- [3] J. Safari and L. Javadian, RSC Adv. 2014, 4, 48973.
- [4] L. Slavov, M.V. Abrashev, T. Merodiiska, Ch. Gelev, R.E. Vandenberghe, I. Markova-Deneva, I. Nedkov, J. Magnetism and Magnetic Materials 2010, 322, 1904.
- [5] Wahajuddin and S. Arora, Int. J. Nanomedicine 2012, 7, 3445.
- [6] J. S. Kim, E. Kuk, K. Nam Yu, J. H. Kim, S. J. Park, H. J. Lee, S. H. Kim, Y. K. Park, Y. H. Park, C.Y. Hwang, Y. K. Kim, Y. S. Lee, D. H. Jeong, M. H. Cho, Nanomedicine: Nanotechnology, Biology and Medicine 2007, 3(1), 95.
- [7] J. R. Postgate, The Sulphate-Reducing Bacteria, 2nd edn. 1984., Cambridge University Press, Newyork.
- [8] H. Mao, J. Feng, X. Ma, C. Wu, X. Zhao, J. Nanopart. Res. 2012, 14, 887.
- [9] M. P. Singh, R. K. Rai and C. Srivastava, ECS Electrochem. Lett. 2014, 3(8), D27.
- [10] M. Knobel, W C Nunes, L M Socolovsky, E De Biasi, J M Vargas, J C Denardin, J. Nanosci. Nanotechnol. 2008, 8(6), 2836.

# Figure captions

- Fig. 1 A schematic showing the arrangement of electrodes in the electrochemical cell.
- Fig. 2 (a) Representative SEM micrograph of Fe<sub>3</sub>O<sub>4</sub>-Ag nanotubes, (b) low and (c) high magnification TEM bright field image of Fe<sub>3</sub>O<sub>4</sub>-Ag nanotubes, (d) an indexed SAD pattern obtained from an agglomerate of nanotubes revealing the presence of Fe<sub>3</sub>O<sub>4</sub> phase, (e) XPS profile obtained from nanotubes revealing Ag<sub>3</sub>d<sub>5/2</sub> and Ag<sub>3</sub>d<sub>3/2</sub> peaks.
- Fig. 3. (a) A representative compositional mapping result and (b) a representative compositional line profile analysis along the nanotube diameter result. Insert in Fig. 3(b) provides the STEM image of the nanowire from which the line profile data was obtained.
- Fig. 4: (a) A representative SEM micrograph of as-deposited Fe<sub>3</sub>O<sub>4</sub> nanotube, (b) low and (c) high magnification TEM bright field image of Fe<sub>3</sub>O<sub>4</sub> nanotubes, (d) an indexed SAD pattern obtained from an agglomerate of nanotubes revealing the presence of Fe<sub>3</sub>O<sub>4</sub> phase (e) result obtained from compositional line profile analysis along the nanotube diameter. Insert in Fig. 4(e) provides the STEM image of the nanowire from which the line profile data was obtained.
- Fig. 5. Magnetic hysteresis loop obtained from as-synthesized (a) Fe<sub>3</sub>O<sub>4</sub>-Ag and (b) Fe<sub>3</sub>O<sub>4</sub> nanotubes.
- Fig. 6: Representative SEM micrograph of (a) Fe<sub>3</sub>O<sub>4</sub>-Ag nanotubes and (b) Fe<sub>3</sub>O<sub>4</sub> nanotube after exposure to SRB.
- Fig. 7: Representative TEM micrograph of (a) Fe<sub>3</sub>O<sub>4</sub>-Ag nanotube and (b) Fe<sub>3</sub>O<sub>4</sub> nanotube after exposure to SRB.

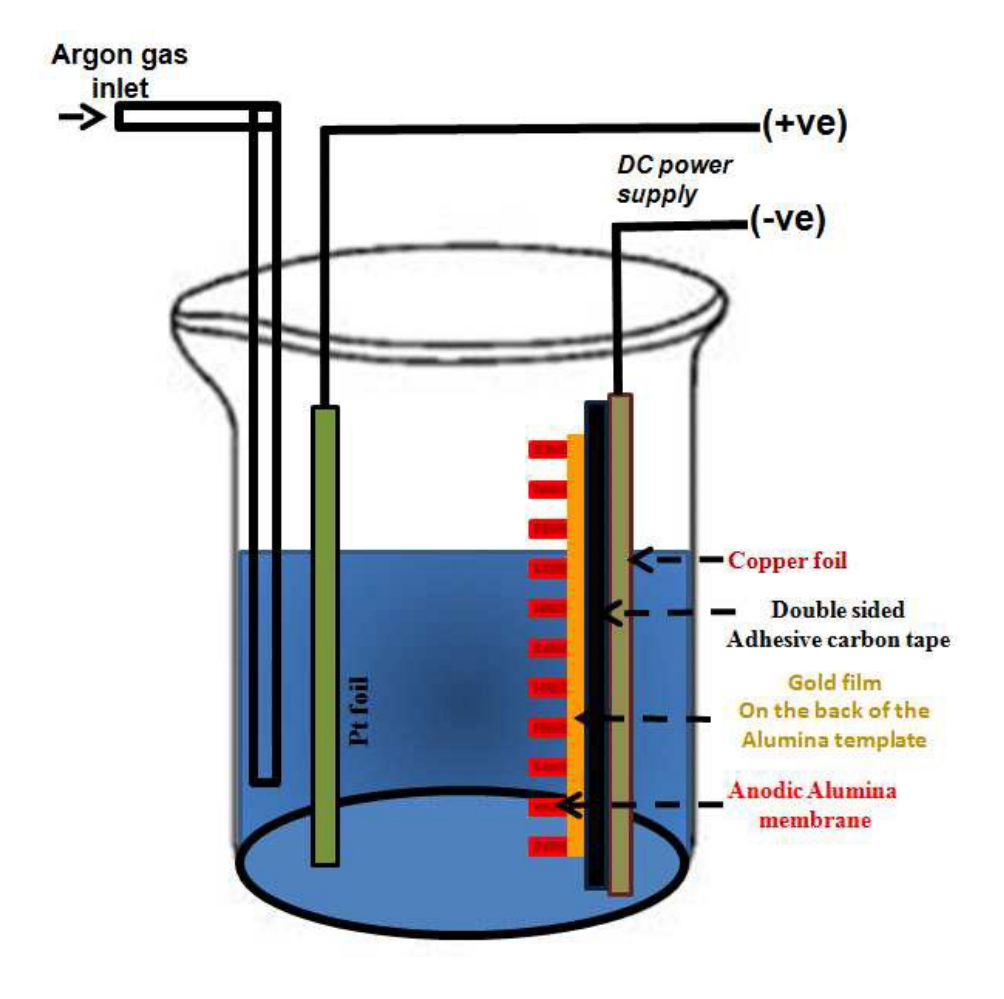


Figure 1

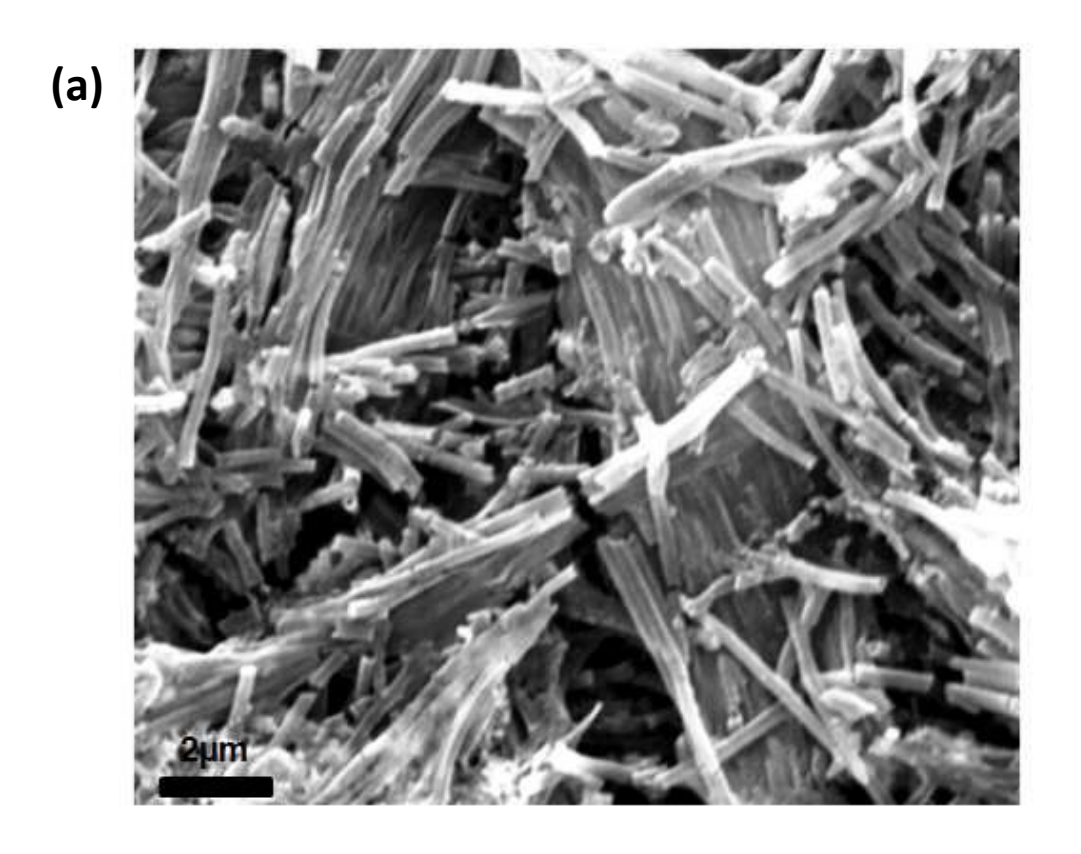
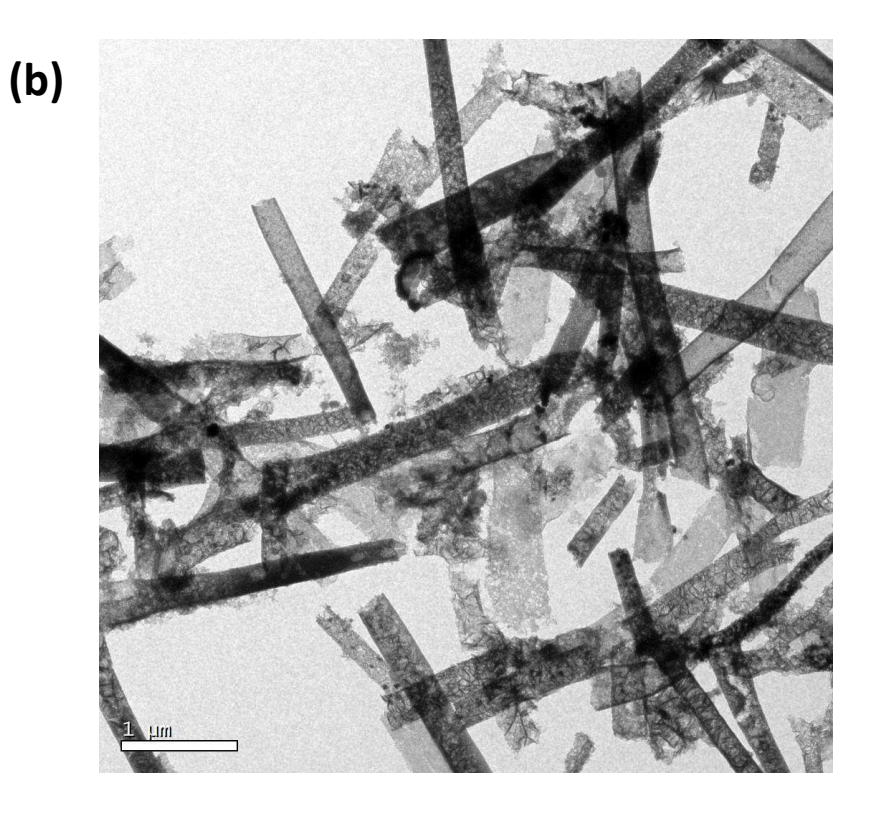


Figure 2



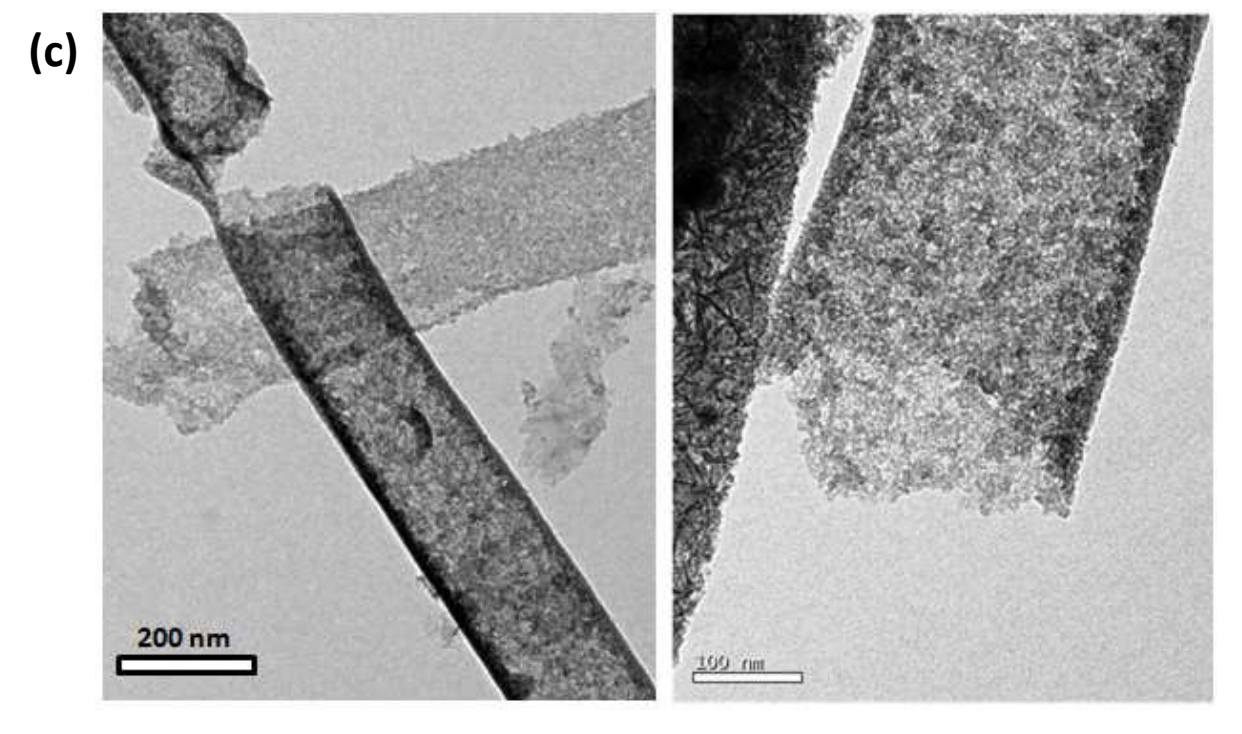
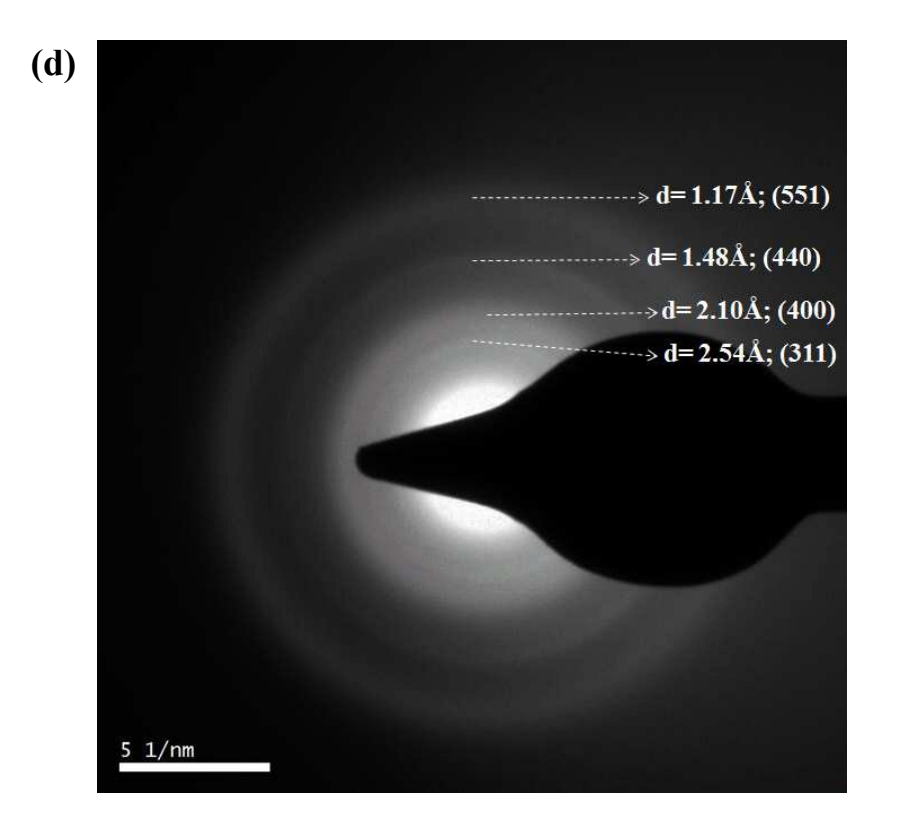


Figure 2



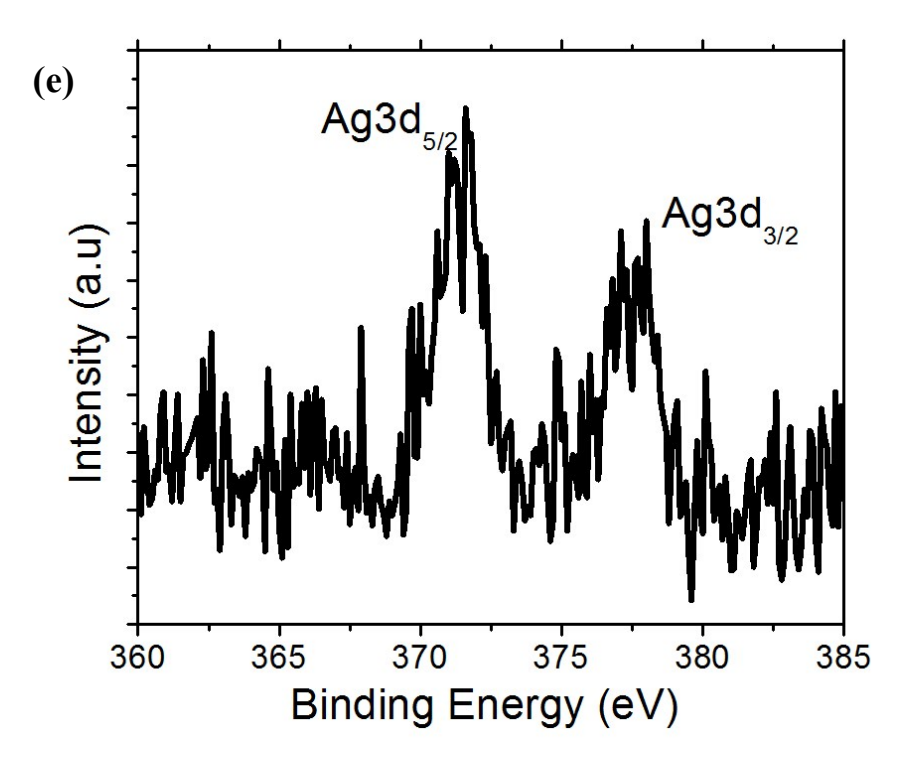
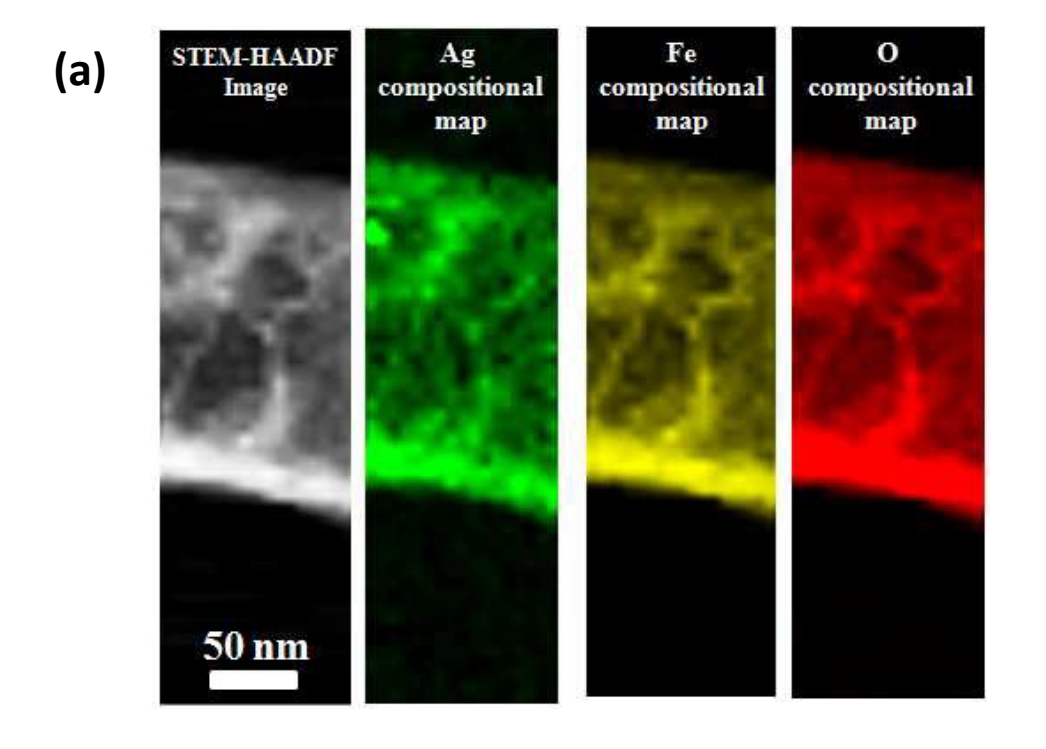


Figure 2



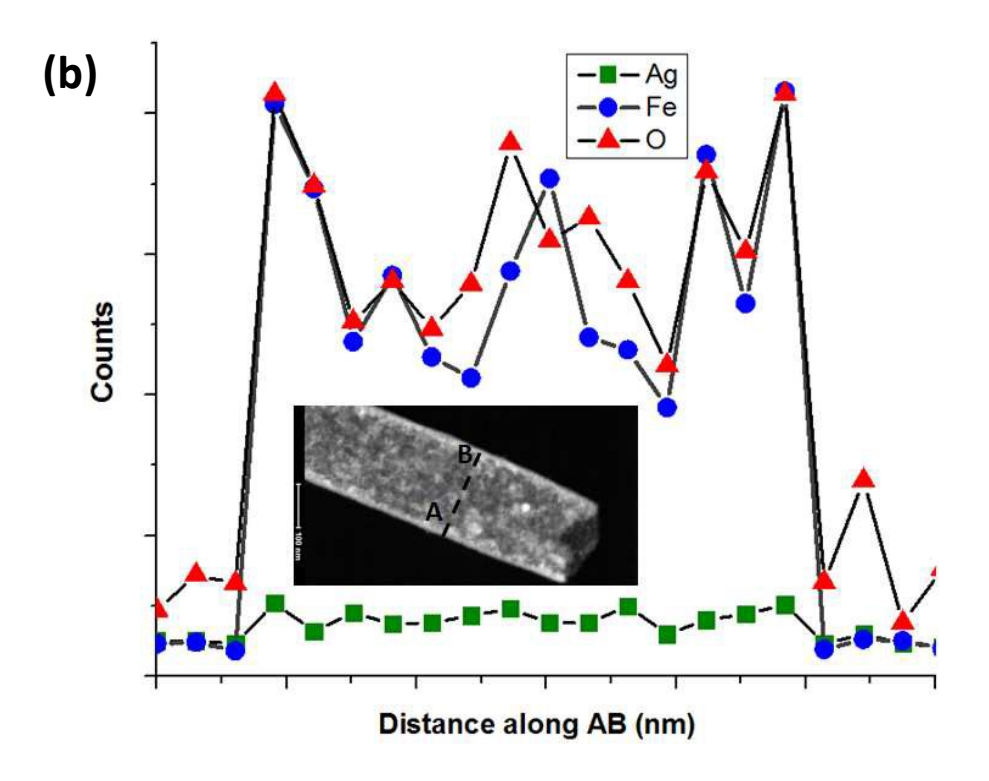
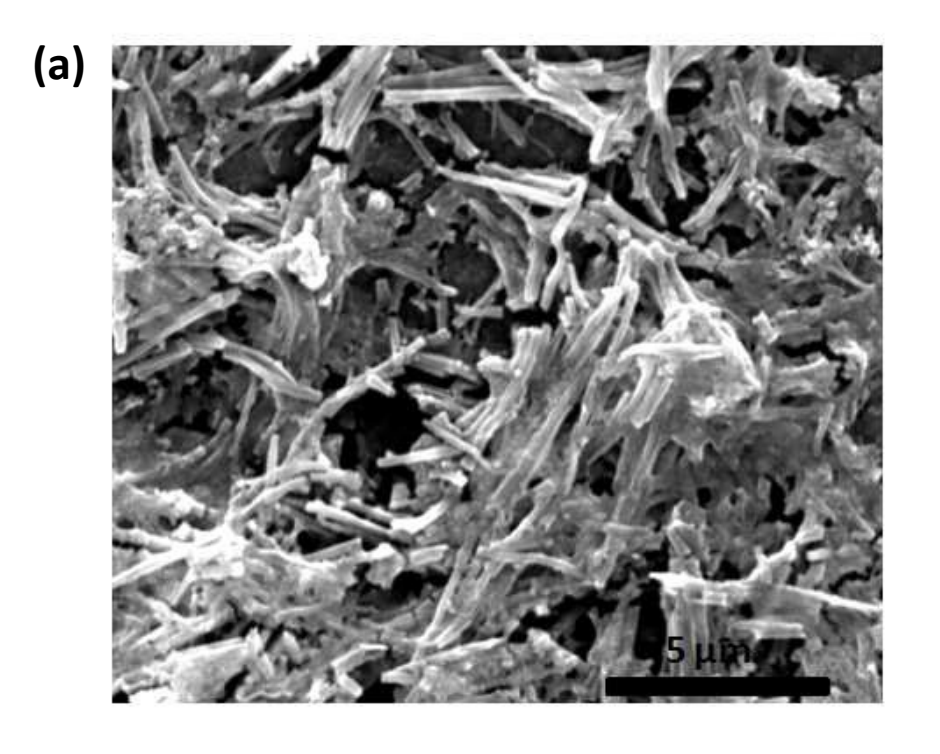


Figure 3



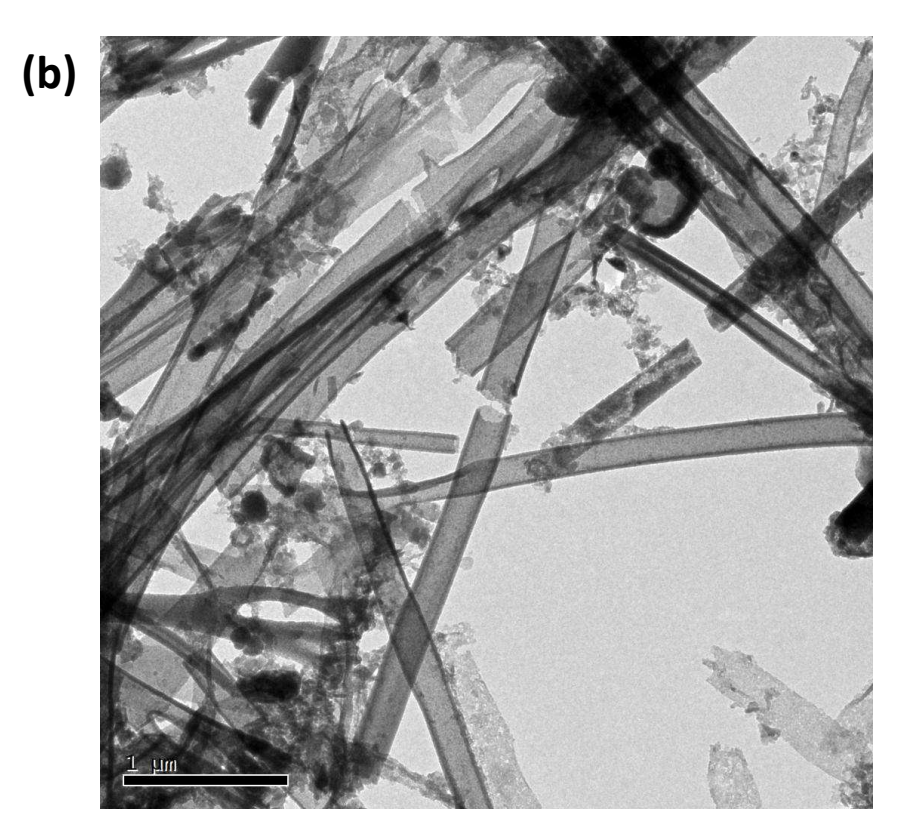
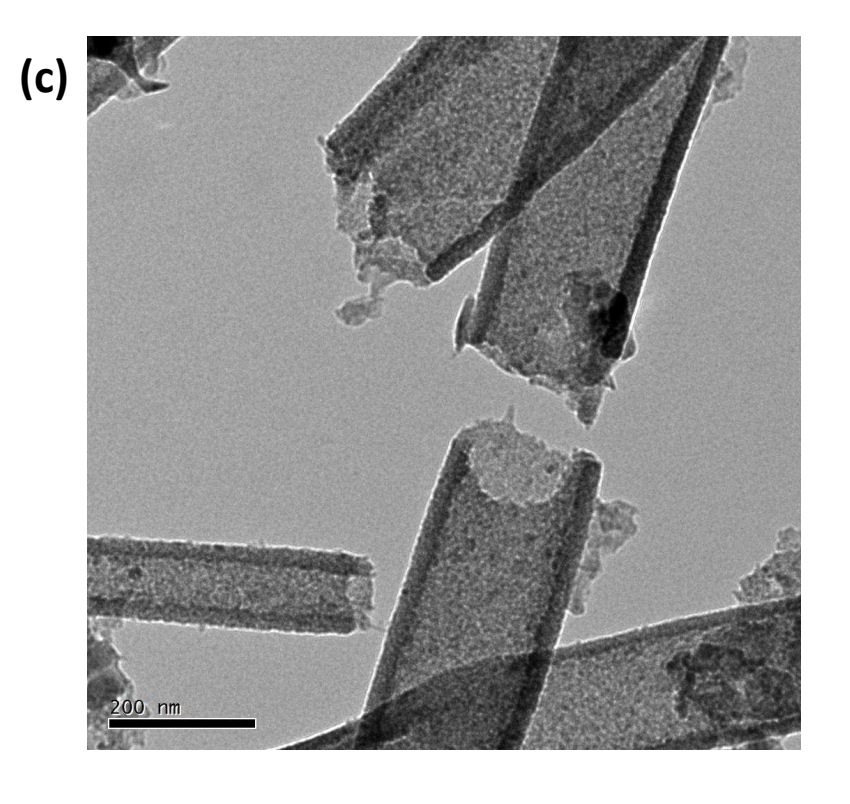


Figure 4



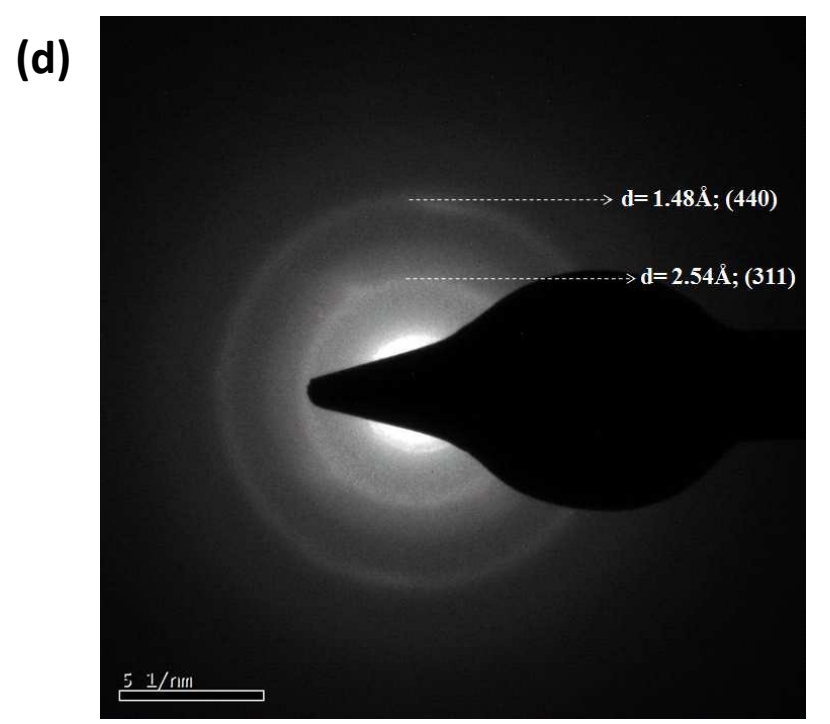


Figure 4

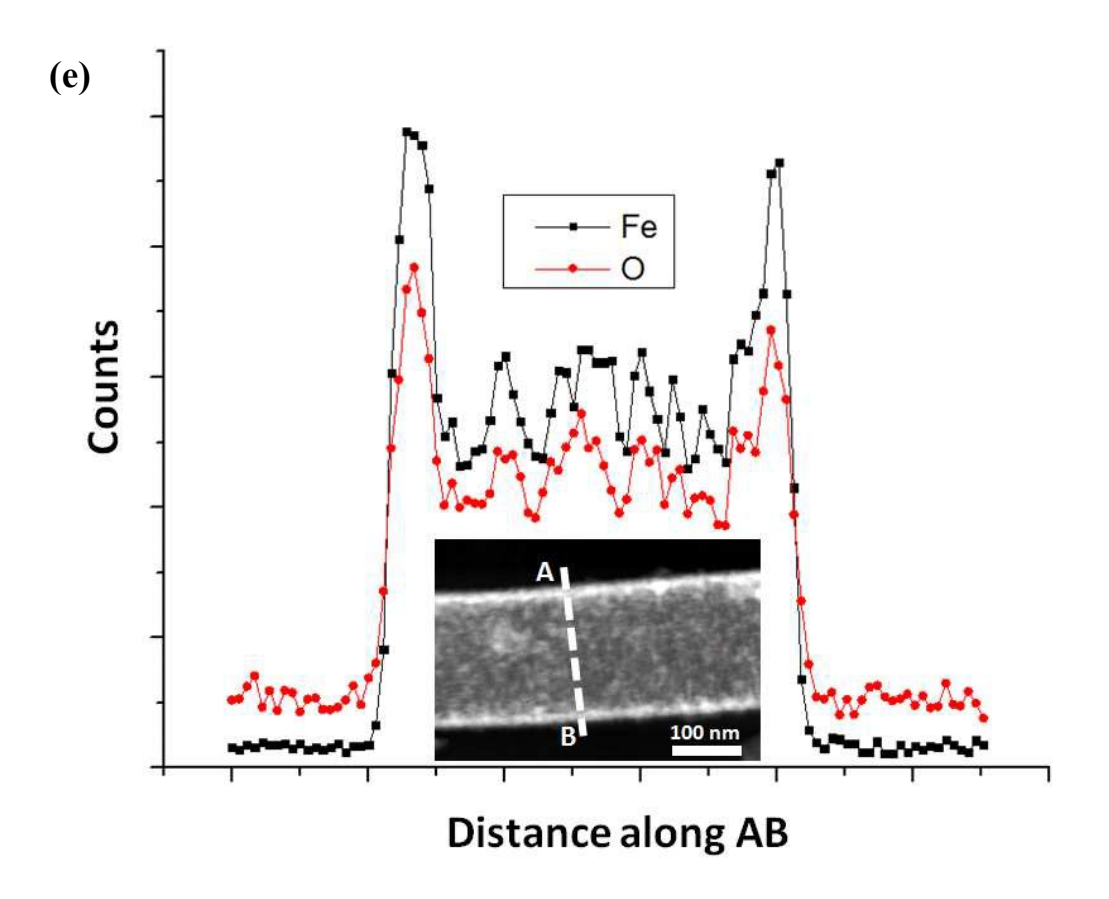
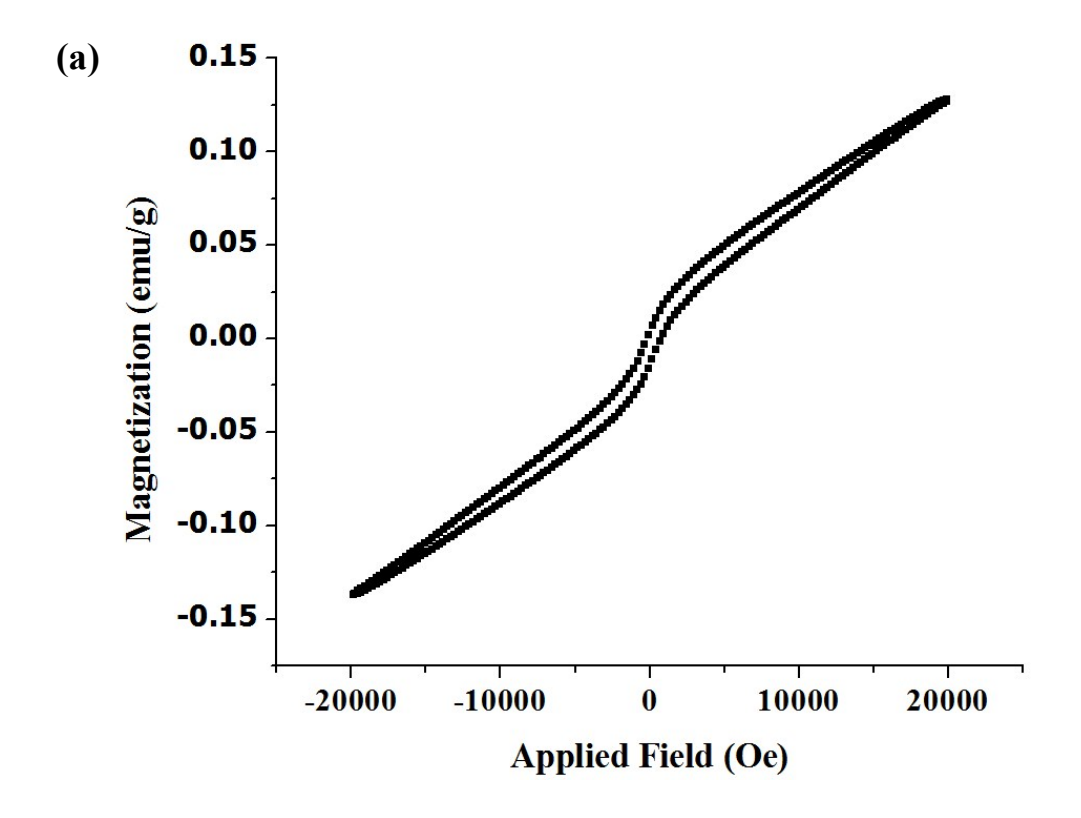


Figure 4



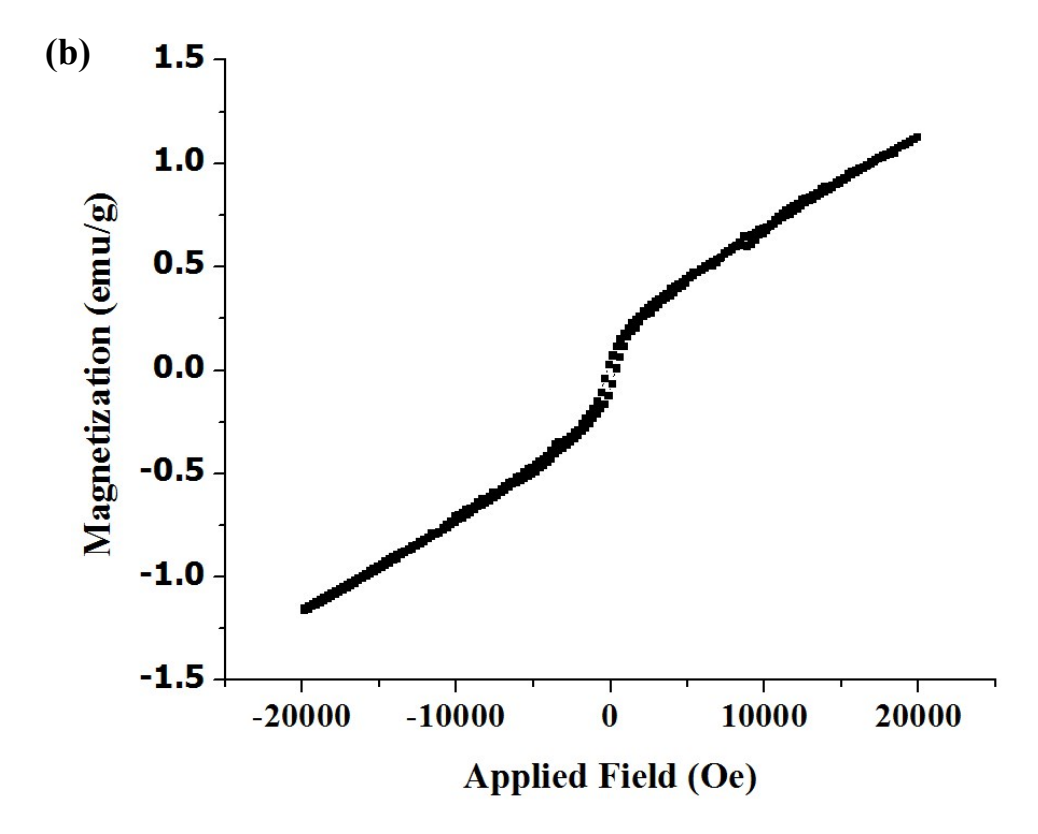
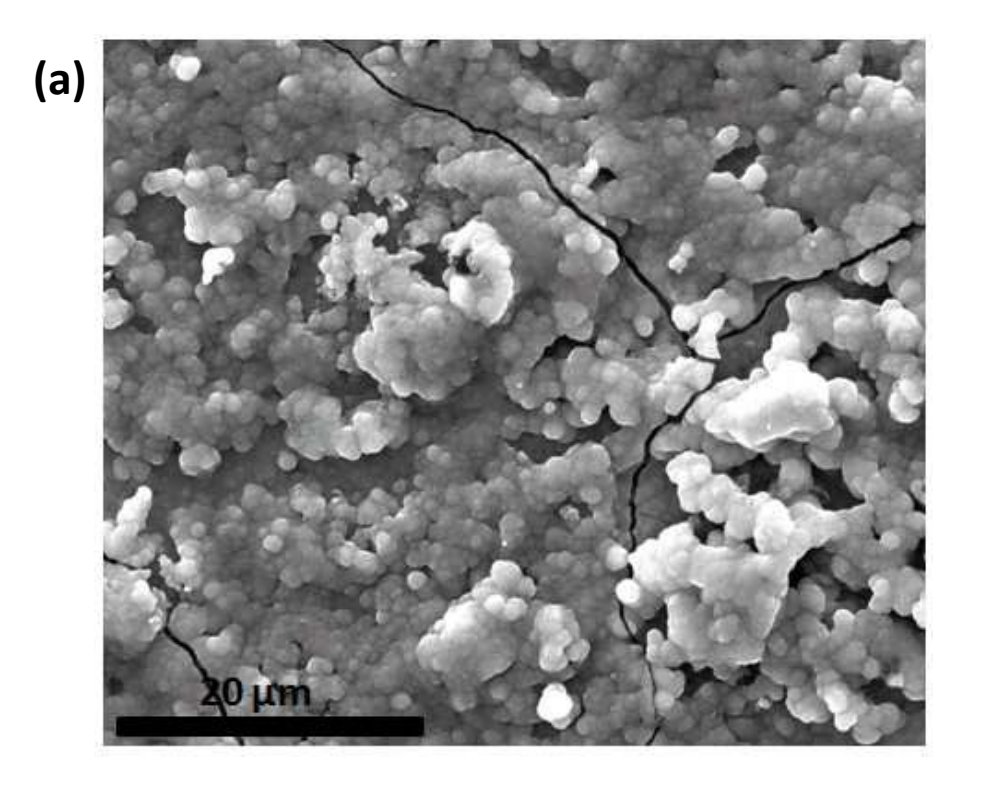


Figure 5



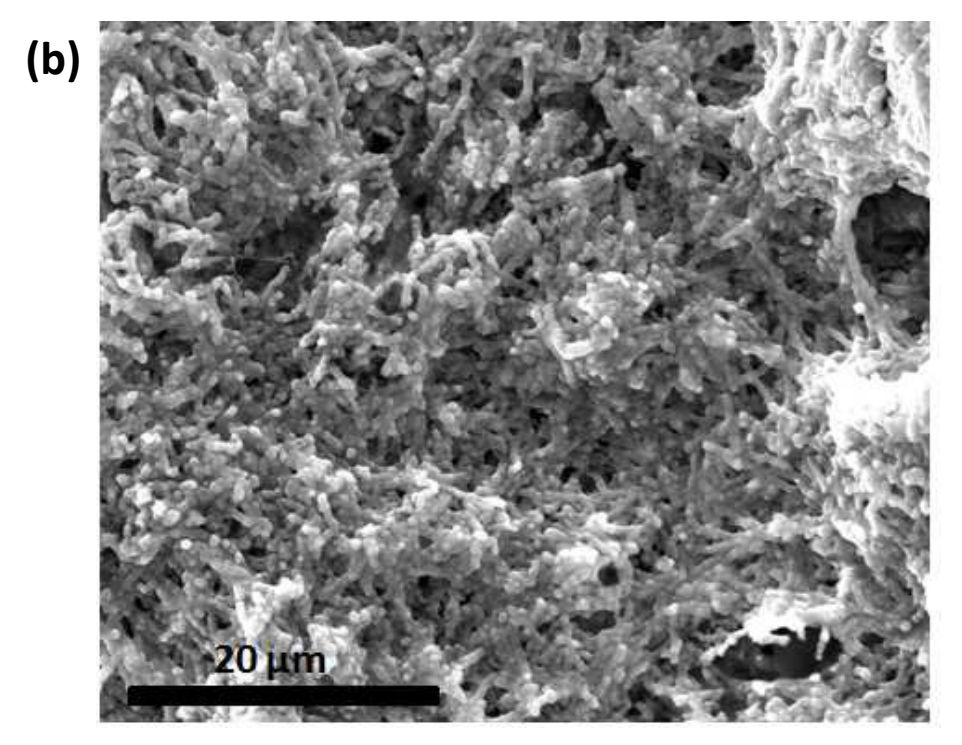
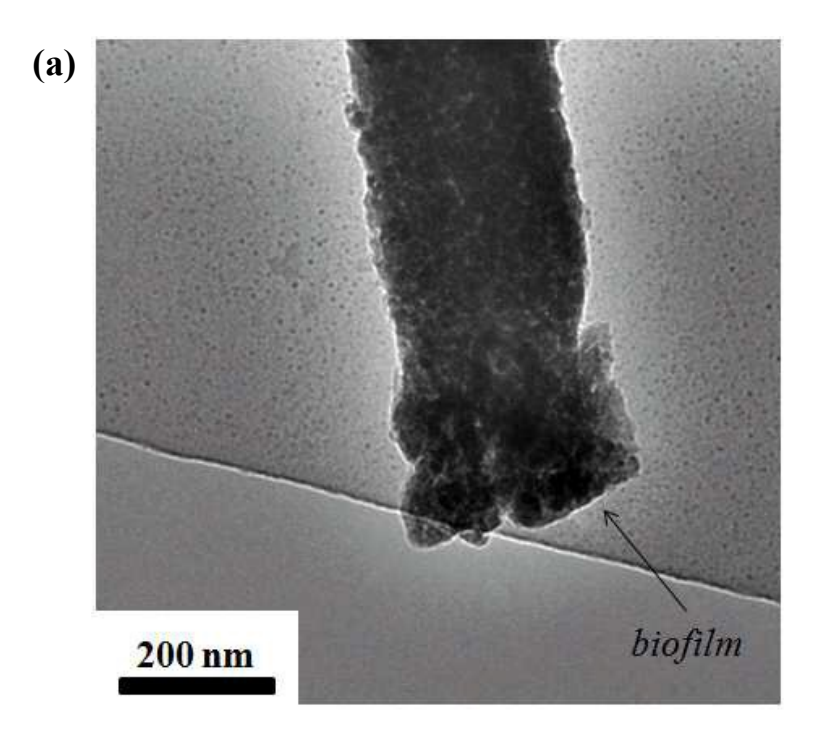


Figure 6



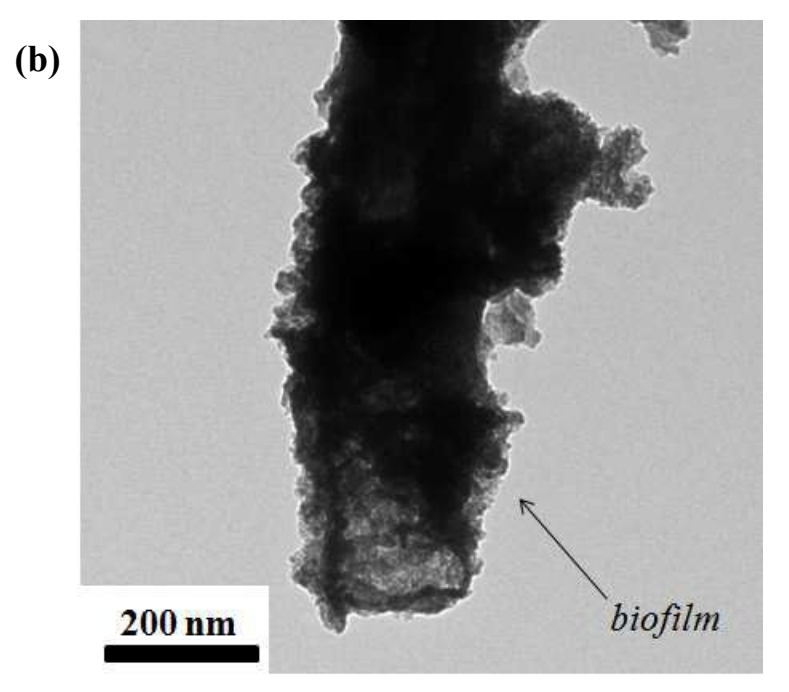


Figure 7